Multivariate Prediction Intervals for Random Forests

Brendan Folie
Citrine Informatics
bfolie@citrine.io

Maxwell Hutchinson
Kiva Microfunds*
maxh@kiva.org

Abstract

Accurate uncertainty estimates can significantly improve the performance of iterative design of experiments, as in Sequential and Reinforcement learning. For many such problems in engineering and the physical sciences, the design task depends on multiple correlated model outputs as objectives and/or constraints. To better solve these problems, we propose a recalibrated bootstrap method to generate multivariate prediction intervals for bagged models and show that it is well-calibrated. We apply the recalibrated bootstrap to a simulated sequential learning problem with multiple objectives and show that it leads to a marked decrease in the number of iterations required to find a satisfactory candidate. This indicates that the recalibrated bootstrap could be a valuable tool for practitioners using machine learning to optimize systems with multiple competing targets.

1 Introduction

Random forest models are typically performant and robust in the small-data regime that characterizes many materials problems, but they lack a natural measure of uncertainty. It is often important to know not just what a model predicts but how confident it is in that prediction. For situations in which a model makes a decision that is of great import to humans, such as who gets a mortgage or who is granted parole [22], an overly-confident model can be disastrous. Accurate uncertainty estimates are also crucial in the physical sciences. For example, a practitioner may be using a model to identify a material that achieves outstanding performance in some application [32]. Directly predicting such performance is beyond the capability of a typical random forest model, but with a well-calibrated uncertainty estimate we may be able to identify candidates that are likely to achieve high performance. For this reason uncertainty estimates are an integral part of machine learning based approaches to experimental design, such as Bayesian Optimization, active and reinforcement learning, and sequential learning [25]. We are especially concerned with multi-objective sequential learning, where the the optimization goal is to find a candidate $\vec{x}$ that meets or exceeds several ambitious design targets $f(\vec{x}) \geq \vec{b}$ for an expensive-to-evaluate vector-valued function f. Sequential learning has been used to identify novel organic LED materials [1, 2], battery materials [39, 20], charging protocols [3], colloidal nanoparticles [14], perovskite photovoltaics [27], and high entropy alloys [34]. More broadly, machine learning-guided experimental design has been used in an astounding variety of fields, including structural engineering [29, 46], public health [4, 8], and transportation [13, 26].

Many real-world problems involve multiple objectives that are strongly related to each other. For example, a scientist may seek to create a new thermoelectric material that efficiently converts waste heat into electricity. This requires high electrical conductivity and low thermal conductivity, but increasing one tends to increase the other. Or a rover may seek to plan a trajectory through space that maximizes the information it collects over the trajectory while minimizing the length of the trajectory [42]. In order to reliably identify promising candidates, a model should be able to produce multivariate prediction intervals that quantify output correlations.

---

[1]Maxwell Hutchinson performed the work while at Citrine Informatics.

Here we propose a <u>multi-output recalibrated bootstrap</u> method to generate multivariate prediction intervals for bagged models by rescaling the bootstrap standard deviation based on the out-of-bag errors. It is fast, easy to implement, and works even with small numbers of bags and training rows. We study the accuracy of the recalibrated bootstrap on a variety of synthetic and real-world test problems, showing that it is well-calibrated. Finally we test the recalibrated bootstrap on a multi-output sequential learning scenario, in which the algorithm attempts to identify a candidate that will simultaneously satisfy several competing objectives. We find a marked decrease in the number of iterations required, which has significant implications for real-world sequential learning.

2 Related Work

Several early and influential studies of uncertainty in random forests focused on generating a confidence interval for the predicted value. Wager et al. [40] studied two generalizations of the jackknife, the infinitesimal jackknife and the jackknife after bootstrap, and introduced a bias-correction term that decreases the number of bags needed for the calculation to converge. Around the same time Mentch and Hooker [31] proposed a modification to the sub-sampling procedure that allows for the generation of confidence intervals. These procedures estimate model variability: by how much is the prediction likely to vary if the model were retrained on a new set of training data drawn from the underlying distribution? **This is not the same as a prediction interval**, which is an attempt to bound the true value. To drive this distinction home, Figure 7 in Appendix E.1 plots the jackknife standard deviation and model error for two one-dimensional test functions and shows that the jackknife can greatly underestimate the true prediction error. Despite this mismatch many works have used the jackknife methods [40] as if they were a prediction interval [36, 41, 37, 7, 25, 24], sometimes leading to sub-optimal results. For example, when using the infinitesimal jackknife to estimate uncertainty as part of a sequential learning study, Rohr et al. [35] take note of the "...general overconfidence of [jackknife-based] methods."

So how does one generate a prediction interval? Quantile Regression Forests (QRF) [30] were an early attempt. A separate model is trained for each desired quantile. QRFs are versatile but require large amounts of data to train and can be noisy [45]. More recently, Lei et al. [23] developed a general "split conformal" method for producing regression prediction intervals. Conformal methods are flexible in that they make no assumptions about the model. They generate prediction intervals by examining the residuals on new test points. The split conformal method reserves some training data for this purpose, hence it is data-inefficient. Dewolf et al. [10] conduct a review of methods to generate prediction intervals on regression problems and find that different methods are better at different problems, but all methods can achieve high accuracy if a conformal method is used to recalibrate the prediction intervals.

Zhang et al. [45] specialized the conformal approach to random forest and made it more efficient by considering the out-of-bag (OOB) residuals. The OOB predictions are those made by base learners that were not exposed to a given training point, and hence they provide a reasonable proxy for how the model will perform on new data points. Zhang et al. [45] prove that their OOB prediction interval has an asymptotically correct coverage rate given certain assumptions. Kim et al. [21], Barber et al. [5] expand on this idea, constructing the prediction intervals using both the OOB residuals and predictions. This allows them to prove bounds on the coverage that are valid even without large amounts of training data. But these approaches are not conditioned on the input, meaning they do not generalize well when the noise is heteroskedastic or the training and test data are not drawn from the same underlying distribution. The lack of conditioning is particularly problematic when designing an experiment (e.g., sequential learning), where the prediction interval should be smaller near previously sampled regions of the domain and larger in unexplored ones.

Lu and Hardin [28] generate a conditional prediction interval by weighting the OOB residuals using a tree-based similarity measure. Another conditional prediction interval is suggested by Palmer et al. [33], who estimate the local uncertainty by calculating the standard deviation over the base learner predictions. This value is shifted and rescaled by constant factors that are estimated based on the residuals computed by cross-validation.

As far as we can tell, the question of multivariate prediction intervals for bagged learners is entirely unexplored in the literature. Our primary contribution is to fill this gap, proposing a method that practitioners can easily use and characterizing it so that they can have confidence in their results.

3 Recalibrated Bootstrap Prediction Intervals

Consider N training examples $Z_i = (\vec{x}_i, \vec{y}_i)$, where $\vec{x}$ is an input vector and $\vec{y}$ is an output vector. The inputs can be of any type but the outputs are real-valued. Assume that the training data are drawn according to some ground-truth function $f(\vec{x})$ with sampling noise parameterized by a distribution $\epsilon(\vec{x})$ that could be heteroskedastic and non-uniform. That is, $\vec{y}_i = f(\vec{x}) + \epsilon(\vec{x})$.

We draw B bootstrap samples of the training data, each of which is generated by sampling N times with replacement. The resulting sample is used to train a base learner that makes predictions on all outputs simultaneously, $\vec{t}_b(\vec{x})$. The model prediction is the mean of the base learners: $\hat{\vec{\theta}}(\vec{x}) = \frac{1}{B} \sum_{b=1}^{B} \vec{t}_b(\vec{x})$. We use a carat to denote a quantity that is estimated over the bootstrap samples.

We propose a prediction interval that is given by a normal distribution centered on $\hat{\vec{\theta}}(\vec{x})$. Though the true interval is not necessarily normal, this approximation is worth considering because it facilitates the generalization to multiple outputs. The only thing that needs to be computed is the covariance matrix of the normal distribution. We take this to be the covariance matrix of the bootstrap predictions, but we rescale each entry using recalibration factors that are computed using the OOB predictions. We use the notation $(-i)$ to determine a quantity computed over the OOB trees for training point i.

We first consider a single response y and show how to generate a standard deviation that corresponds to a normal prediction interval. We choose a confidence level parameter $p \in (0, 1)$ and calculate the equivalent number of standard deviations of a normal distribution: $\eta(p) = \Phi^{-1}(\frac{1+p}{2})$ where Φ is the CDF of a unit normal distribution. Given p, Algorithm 1 describes how to calculate the recalibration factor α and apply it to new predictions.

Algorithm 1: Recalibrated Bootstrap Prediction Interval in One Dimension

---

Stage : Determine recalibration factor α_p;
Given : N training points $(\vec{x}_i, y_i)$ used to generate B bootstrap samples and base learners $t_b(\vec{x})$;
Given : A confidence level parameter, $p \in (0, 1)$;
for all training points $\vec{x}_i$ **do**

> Calculate the out-of-bag mean and standard deviation, $\hat{\theta}_{(-i)}(\vec{x})$ and $\hat{s}_{(-i)}(\vec{x})$;
>
> Calculate the out-of-bag standard residual, $|\tilde{r}_{oob}| = \dfrac{|\hat{\theta}_{(-i)}(\vec{x}) - y_i|}{\hat{s}_{(-i)}}$;

end
Let $\tilde{r}_p$ be the p-percentile value of the $|\tilde{r}_{oob}|$;
Set $\alpha = \tilde{r}_p / \eta(p)$, where $\eta(p)$ is the equivalent number of standard deviations of a normal distribution;
Stage : Estimate prediction interval for a new input;
Given : new input $\vec{x}$;
Calculate $\hat{s}(\vec{x})$, the standard deviation over the predictions $t_b(\vec{x})$;
The prediction interval is a normal distribution with mean $\hat{\theta}(\vec{x})$ and standard deviation $\alpha * \hat{s}(\vec{x})$

Like Palmer et al. [33], this method computes factors to recalibrate the bootstrap standard deviation. But there are two key differences. First, using the OOB residuals instead of cross-validation makes the method more data-efficient. Second, as we will show in the subsequent analysis, using the p-percentile instead of the maximum likelihood estimate (MLE) makes the method more robust to outliers as long as the chosen value of p is not too extreme.

The generalization to a multivariate prediction interval is straight-forward. For each pair of outputs we calculate a recalibrated covariance using the individual recalibration factors. Let α_j and α_k be the recalibration factors for outputs j and k. For a given output j let $t_{bj}(\vec{x})$ be the prediction of tree b, $\hat{\theta}_j(\vec{x})$ be the mean prediction, and $\hat{\sigma}_j(\vec{x})$, written explicitly in Equation 1, be the recalibrated standard deviation that forms the univariate prediction interval.

$$\hat{\sigma}_j(\vec{x}) = \alpha_j \sqrt{\frac{1}{B-1} \sum_{b=1}^{B} (t_{bj}(\vec{x}) - \hat{\theta}_j(\vec{x}))^2} \tag{1}$$

The covariance estimate is then given by Equation 2,

$$\hat{\sigma}_{jk}^2 = \frac{1}{B-1} \sum_{b=1}^{B} \Big(\alpha_j(t_{bj}(\vec{x}) - \hat{\theta}_j(\vec{x})) \Big) \Big(\alpha_k(t_{bk}(\vec{x}) - \hat{\theta}_k(\vec{x})) \Big) = \hat{\rho}_{jk}(\vec{x})\hat{\sigma}_j(\vec{x})\hat{\sigma}_k(\vec{x}), \quad (2)$$

where $\hat{\rho}_{jk}(\vec{x})$ is the Pearson correlation coefficient over the tree-wise predictions. If the resulting covariance matrix is $\hat{\Sigma}(\vec{x})$ then the predictive distribution is normal: $\mathcal{N}(\hat{\vec{\theta}}(\vec{x}), \hat{\Sigma}(\vec{x}))$.

This is a pleasing result – by making the predictive distribution normal and using the tree-wise standard deviation as a proxy for uncertainty, we arrive at a multivariate distribution that is nearly free to evaluate and is fully describes a multivariate prediction interval without large amounts of training data. Other methods to compute a prediction interval, such as Zhang et al. [45] or Lu and Hardin [28], are parameter-free but do not have a clear multivariate generalization, and any such generalization would likely require the amount of data to grow exponentially with the number of outputs.

Subsequent sections will show that this predictive distribution is well calibrated and leads to more efficient sequential learning. In Appendix B.1 we consider the parameter p and show that it has little effect on the results, so we set $p = 0.683$ (one standard deviation) for the rest of the manuscript. We also show in B.3 that the standard OOB residuals can be assumed to come from the same distribution as the test set residuals and in B.4 that the bootstrap variance is proportional to the true squared residual. The underlying assumptions are expected to be less valid for real-world data sets, but as we show in this work, the recalibrated bootstrap is robust in the presence of real, skewed data.

4 How Well Calibrated is the Recalibrated Bootstrap?

We perform numerical experiments to investigate the accuracy of the recalibrated bootstrap method. The real-world and synthetic data sets used are described in Appendix A. For each test problem we generate training and test data sets, train a model with the package Lolo [19], apply the model to the test data, and evaluate the performance of the proposed prediction intervals by comparing them to the "observed" values. More details can be found in Appendix C. All of the figures, numerical results, data sets, and code are available at `https://github.com/CitrineInformatics/multivariate-prediction-intervals`.
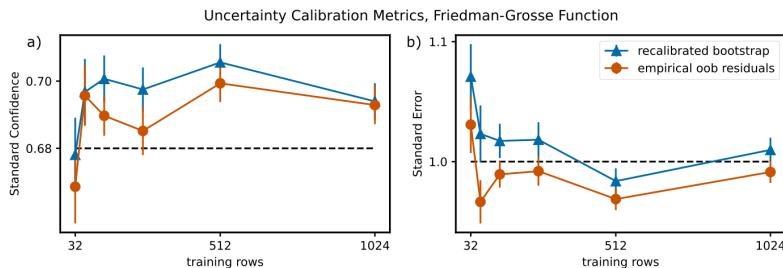
Figure 1: The recalibrated bootstrap produces a well-calibrated univariate prediction interval on synthetic data, as seen by examining a) standard confidence and b) standard error (dashed lines are the ideal values). The empirical OOB residuals method [45] also performs well on this problem. Data are generated using the Friedman-Grosse function with normally distributed noise of magnitude 2.0. There are 128 test points. 64 trials were run, each involving a different set of training and test data. Error bars show one standard error.

Figure 1 shows the standard confidence and standard error (Appendix C.1) for test data generated using the Friedman-Grosse function. We compare the recalibrated bootstrap to the non-parametric "empirical OOB residuals" method [45]. Both methods are well calibrated. We consider other test problems, including more skewed real-world data, in Figure 9 In Appendix E.2 we consider what happens when the test and training sets are drawn from highly divergent distributions. The recalibrated bootstrap is found to be robust, but the method of Zhang et al. [45] becomes over-confident as the test set grows more difficult.

4

Performance on multivariate problems is shown in Figure 6. The recalibrated bootstrap is consistently well calibrated and the MNLPD (Appendix C.1) is overall better than the other methods we considered.

5   Application to Multi-Objective Sequential Learning

A lower MNLPD value is all well and good, but what we really want to know is whether or not this predictive distribution can help us make better decisions. We consider sequential learning (SL), a type of active learning, as a test problem [25]. A user attempts to find an input point $\vec{x}$ that leads to output $\vec{y}$ that simultaneously satisfies all objectives. Given initial training data, we train a multi-output random forest model. The model makes predictions at all unknown points, and an acquisition function is used to evaluate the suitability of some test point. The highest-scoring test point is chosen for measurement. If it satisfies the objectives then we are done. If not then it is added to the training set and the cycle repeats. This is similar in practice to Bayesian Optimization [38], but with a non-Bayesian model for the objectives and an acquisition function defined only on the posterior distribution of the predictions.
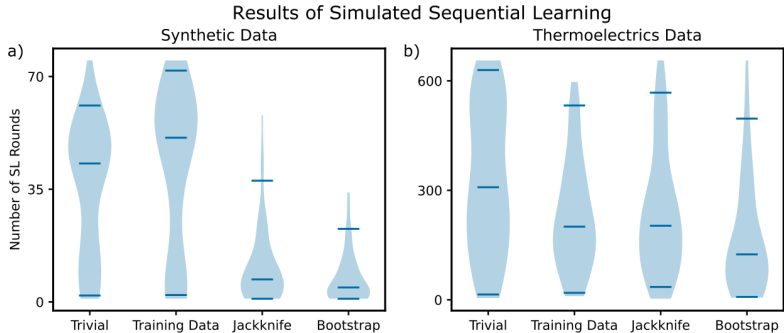
Figure 2: Violin plots showing the distribution of the number of rounds required to find a satisfactory candidate for the a) synthetic and b) thermoelectrics problem show the distribution of the number of rounds required to find a satisfactory candidate. Lines indicate the 5th percentile, median, and 95th percentile. The recalibrated bootstrap method is the most efficient of the methods considered. 64 independent trials were performed.

Details of the two simulated SL problems are in Appendix C.4 and results are shown in Figure 2 and Table 1 (Appendix C.5). The recalibrated bootstrap consistently requires the fewest iterations to find a satisfactory candidate. Compared to the trivial method, the median trial requires 90% fewer iterations for the synthetic problem and 60% fewer iterations for the thermoelectrics problem. Perhaps more importantly, the trivial method suffers from a long tail of disastrous trials in which the performance is worse than that of random guessing. The recalibrated bootstrap largely avoids this pathology.

6   Conclusions

We propose a "recalibrated bootstrap" method to generate multivariate prediction intervals for random forest or any other bagged ensemble model. The covariance matrix of the bootstrap predictions defines a multivariate normal distribution, but the entries are rescaled using the out-of-bag residuals. We show that this prediction interval is well-calibrated by testing it against several data sets.

Our focus is not, however, the prediction interval itself, but its applicability to multi-output sequential learning (SL). We simulate SL and show that using the recalibrated bootstrap significantly decreases the number of iterations required to find a high-performing candidate by between 2x and 8x compared to common alternatives. Although this study is limited in that it only considers a few data sets, we feel that the dramatic improvement seen on real-world, noisy, imbalanced data is promising enough to merit its use and further study.

Developing the next-generation materials crucial to renewable energy generation and storage is an ideal problem for multi-objective SL: there are typically multiple ambitious goals that compete against each other, existing data sets are modest in size, and each experiment can be enormously expensive. The recalibrated bootstrap can be a powerful tool for making AI-guided design more efficient.

References

[1] Hadi Abroshan, Anand Chandrasekaran, Paul Winget, Yuling An, Shaun Kwak, Christopher Brown, and Mathew D. Halls. Accelerated design and optimization of novel oled materials via active learning. SPIE Organic Photonics and Electronics, 11808, 2021.

[2] Erin Antono, Nobuyuki N. Matsuzawa, Julia Ling, James Edward Saal, Hideyuki Arai, Masaru Sasago, and Eiji Fujii. Machine-learning guided quantum chemical and molecular dynamics calculations to design novel hole-conducting organic materials. Journal of Physical Chemistry A, 124(40):8330–8340, 2020.

[3] Peter M. Attia, Aditya Grover, Norman Jin, Kristen A. Severson, Todor M. Markov, Yang-Hung Liao, Michael H. Chen, Bryan Cheong, Nicholas Perkins, Zi Yang, Patrick K. Herring, Muratahan Aykol, Stephen J. Harris, Richard D. Braatz, Stefano Ermon, and William C. Chueh. Closed-loop optimization of fast-charging protocols for batteries with machine learning. Nature, 578:397–402, 2020.

[4] Abdul Awal, Mehedi Masud, Shahadat Hossain, Abdullah Al-Mamun Bulbul, Hasan Mahmud, and Anupam Kumar Bairagi. A novel bayesian optimization-based machine learning framework for covid-19 detection from inpatient facility data. IEEE Access, 9:10263–10281, 2021.

[5] Rina Foygel Barber, Emmanuel J. Candes, Aaditya Ramdas, and Ryan J. Tibshirani. Predictive inference with the jackknife+. Annals of Statistics, 49:486–507, 2021.

[6] Christopher K. H. Borg, Carolina Frey, Jasper Moh, Tresa M. Pollock, Stéphane Gorsse, Daniel B. Miracle, Oleg N. Senkov, Bryce Meredig, and James E. Saal. Expanded dataset of mechanical properties and observed phases of multi-principal element alloys. Scientific Data, 7, 2020.

[7] Ernesto Carrella. No free lunch when estimating simulation parameters. The Journal of Artificial Societies and Social Simulations, 24, 2021.

[8] Amit Chandak, Debojyoti Dey, Bhaskar Mukhoty, and Purushottam Kar. Epidemiologically and socio-economically optimal policies via bayesian optimization. Transactions of the Indian National Academy of Engineering, 5:117–127, 2020.

[9] Zachary del Rosario, Matthias Rupp, Yoolhee Kim, Erin Antono, and Julia Ling. Assessing the frontier: Active learning, model accuracy, and multi-objective candidate discovery and optimization. The Journal of Chemical Physics, 153, 2020.

[10] Nicolas Dewolf, Bernard De Baets, and Willem Waegeman. Valid prediction intervals for regression problems. ArXiv, 2021. doi: arXiv:2017.00363v2.

[11] Bradley Efron. The jackknife, the bootstrap, and other resampling plans. The Society for Industrial and Applied Mathematics, 1982.

[12] Bradley Efron. Estimation and accuracy after model selection. Journal of the American Statistical Association, 109, 2014.

[13] Fatemeh Fakhrmoosavi, Ehsan Kamjoo, Mohammadreza Kavianipour, Ali Zockaie, Alireza Talebpour, and Archak Mittal. A stochastic framework using bayesian optimization algorithm to assess the network-level societal impacts of connected and autonomous vehicles. Transportation Research Part C: Emerging Technologies, 139, 2022.

[14] Anthony Y. Fong, Lenson Pellouchoud, Malcolm Davidson, Richard C. Walroth, Carena Church, Ekaterina Tcareva, Liheng Wu, Kyle Peterson, Bryce Meredig, and Christopher J. Tassone. Utilization of machine learning to accelerate colloidal synthesis and discovery. The Journal of Chemical Physics, 154, 2021.

[15] J. H. Friedman and B. W. Silverman. Flexible parsimonious smoothing and additive modeling. Technometrics, 3:3–39, 1989.

[16] J. H. Friedman, E. Grosse, and W. Stuetzle. Multidimensional additive spline approximation. SIAM J. Sci. Statist. Comput., 4:291–301, 1983.

[17] Michael W. Gaultois, Taylor D. Sparks, Christopher K. H. Borg, Ram Seshadri, William D. Bonificio, and David R. Clarke. Data-driven review of thermoelectric materials: Performance and resource considerations. Chemistry of Materials, 25(15):2911–2920, 2013.

[18] Indrayudh Ghosal. Model Combinations and the Infinitesimal Jackknife: How to Refine Models With Boosting and Quantify Uncertainty. PhD thesis, Cornell University, 2021.

[19] Maxwell Hutchinson. Lolo. https://github.com/CitrineInformatics/lolo, 2016.

[20] Adarsh Dave Jared Mitchell Kirthevasan Kandasamy, Han Wang Sven Burke, Biswajit Paria, Barnabás Póczos, Jay Whitacre, and Venkatasubramanian Viswanathan. Autonomous discovery of battery electrolytes with robotic experimentation and machine learning. Cell Reports Physical Science, 1, 2020.

[21] Byol Kim, Chen Xu, and Rina Foygel Barber. Predictive inference is free with the jackknife+-after-bootstrap. NeurIPS, 34, 2020.

[22] Arun K. Kuchibhotla and Richard A. Berk. Nested conformal prediction sets for classification with applications to probation data. ArXiv, 2021. doi: arXiv:2104.09358v1.

[23] Jing Lei, Max G'Sell, Alessandro Rinaldo, Ryan J. Tibshirani, and Larry Wasserman. Distribution-free predictive inference for regression. Journal of the American Statistical Association, 113:1094–1111, 2018.

[24] Jean-Marie Lepioufle, Leif Marsteen, and Mona Johnsrud. Error prediction of air quality at monitoring stations using random forest in a total error framework. Physical Sensors, 21, 2021.

[25] Julia Ling, Maxwell Hutchinson, Erin Antono, Sean Paradiso, and Bryce Meredig. High-dimensional materials and process optimization using data-driven experimental design with well-calibrated uncertainty estimates. Integrating Materials and Manufacturing Innovation, 6: 207–217, 2017.

[26] Renming Liu, Yu Jiang, and Carlos Lima Azevedo. Bayesian optimization of area-based road pricing. International Conference on Models and Technologies for Intelligent Transportation Systems, 7, 2021.

[27] Zhe Liu, Nicholas Rolston, Austin C. Flick, Thomas W. Colburn, Zekun Ren, Reinhold H. Dauskardt, and Tonio Buonassisi. Machine learning with knowledge constraints for process optimization of open-air perovskite solar cell manufacturing. ArXiv, 2022. doi: arXiv:2110.01387v4.

[28] Benjamin Lu and Johanna Hardin. A unified framework for random forest prediction error estimation. Journal of Machine Learning Research, 22:1–41, 2021.

[29] Alexandre Mathern, Olof Skogby Steinholtz, Anders Sjöberg, Magnus Önnheim, Kristine Ek, Rasmus Rempling, Emil Gustavsson, and Mats Jirstrand. Multi-objective constrained bayesian optimization for structural design. Structural and Multidisciplinary Optimization, 63:689–701, 2021.

[30] Nicolai Meinshausen. Quantile regression forests. Journal of Machine Learning Research, 7: 983–999, 2006.

[31] Lucas Mentch and Giles Hooker. Quantifying uncertainty in random forests via confidence intervals and hypothesis tests. Journal of Machine Learning Research, 17:1–41, 2016.

[32] Bryce Meredig, Erin Antono, Carena Church, Maxwell Hutchinson, Julia Ling, Sean Paradiso, Ben Blaiszik, Ian Foster, Brenna Gibbons, Jason Hattrick-Simpers, Apurva Mehta, and Logan Ward. Can machine learning identify the next high-temperature superconductor? examining extrapolation performance for materials discovery. Molecular Systems Design and Engineering, 3:819 – 825, 2018.

[33] Glenn Palmer, Siqi Du, Alexander Politowicz, Joshua Paul Emory, Xiyu Yang, Anupraas Gautam, Grishma Gupta, Zhelong Li, Ryan Jacobs, and Dane Morgan. Calibrated bootstrap for uncertainty quantification in regression models. ArXiv, 2021. doi: arXiv:2105.13303v1.

[34] Ziyuan Rao, PoYen Tung, Ruiwen Xie, Ye Wei, Hongbin Zhang, Alberto Ferrari, T.P.C. Klaver, Fritz Körmann, Prithiv Thoudden Sukumar, Alisson Kwiatkowski da Silva, Yao Chen, Zhiming Li, Dirk Ponge, Jörg Neugebauer, Oliver Gutfleisch, Stefan Bauer, and Dierk Raabe. ArXiv, 2022. doi: arXiv:2202.13753.

[35] Brian Rohr, Helge S. Stein, Dan Guevarra, Yu Wang, Joel A. Haber, Muratahan Aykol, Santosh K. Suram, and John M. Gregoire. Benchmarking the acceleration of materials discovery by sequential learning. Chemical Science, 11:2696–2706, 2020.

[36] Darius Roman, Saurabh Saxena, Valentin Robu, Michael Pecht, and David Flynn. Machine learning pipeline for battery state-of-health estimation. Nature Machine Intelligence, 3:447–456, 2021.

[37] Alexander Ruesch, Jason Yang, Samantha Schmitt, Deepshikha Acharya, Matthew A. Smith, and Jana M. Kainerstorfer. Estimating intracranial pressure using pulsatile cerebral blood flow measured with diffuse correlation spectroscopy. Biomedical Optics Express, 11(3), 2020.

[38] Bobak Shahriari, Kevin Swersky, Ziyu Wang, Ryan P. Adams, and Nando de Freitas. Taking the human out of the loop: A review of bayesian optimization. Proceedings of the IEEE, 104 (1), 2016.

[39] Juan C. Verduzco, Ernesto E. Marinero, and Alejandro Strachan. An active learning approach for the design of doped llzo ceramic garnets for battery applications. Integrating Materials and Manufacturing Innovation, 10:299–310, 2021.

[40] Stefan Wager, Trevor Hastie, and Bradley Efron. Confidence intervals for random forests: The jackknife and the infinitesimal jackknife. Journal of Machine Learning Research, 15: 1625–1651, 2014.

[41] Hud Wahab, Vivek Jain, Alexander Scott Tyrrell, Michael Alan Seas, Lars Kotthoff, and Patrick Alfred Johnson. Machine-learning-assisted fabrication: Bayesian optimization of laser-induced graphene patterning using in-situ raman analysis. Carbon, 167:609–619, 2020.

[42] Z. Wang, C. Gehring, P. Kohli, and S. Jegelka. Batched large-scale bayesian optimization in high-dimensional spaces. Proceeding of Machine Learning Research, 84:745 – 754, 2018.

[43] L. Ward, A. Dunn, A. Faghaninia, N. E. R. Zimmermann, S. Bajaj, J. H. Wang, Q.and Montoya, J. Chen, K. Bystrom, M. Dylla, K. Chard, M. Asta, K. Persson, G. J. Snyder, I. Foster, and A. Jain. Matminer: An open source toolkit for materials data mining. Computational Materials Science, 152:60–69, 2018.

[44] Logan Ward, Ankit Agrawal, Alok Choudhary, and Christopher Wolverton. A general-purpose machine learning framework for predicting properties of inorganic materials. npj Computational Materials, 2, 2016.

[45] Haozhe Zhang, Joshua Zimmerman, Dan Nettleton, and Daniel J. Nordman. Random forest prediction intervals. The American Statistician, 74:392–406, 2020.

[46] Yi-Ming Zhang, Hao Wang, Jian-Xiao Mao, Zi-Done Xu, and Yu-Feng Zhang. Probabilistic framework with bayesian optimization for predicting typhoon-induced dynamic responses of a long-span bridge. Journal of Structural Engineering, 147, 2021.

A Compendium of Test Problems

The sections below describe how to generate ground-truth data for each test problem. For synthetic problems additional noise may be added in the form of $\epsilon * \mathcal{N}(0, 1)$, where ϵ is the noise level.

A.1 Tophat

The tophat method used in Figure 7a is defined in Equation 3.

$$y = \begin{cases} 1.0, & \text{if } |x| < 0.33 \\ 0.5, & \text{if } 0.33 \le |x| < 0.67 \\ 0, & \text{otherwise} \end{cases} \tag{3}$$

A.2 Cubic

The cubic method used in Figure 7b is simply $y = x^3$.

A.3 Friedman-Grosse

The Friedman-Grosse function [16], in Equation 4 is defined on the unit hypercube in at least 5 dimensions. In this paper we use 8 dimensions, but dimensions 6-8 do not contribute to the output.

$$y_0 = 10 \sin(\pi x_0 x_1) + 20(x_2 - 0.5)^2 + 10x_3 + 5x_4 \tag{4}$$

A.3.1 Additional Outputs for Calibration Studies

For the purposes of investigating the predictive distribution's calibration (Figure 6) we generate two additional outputs, both of which are correlated with Y_0. The first additional output, Y_1, has some fixed linear correlation, ρ, with Y_0. The second additional output, Y_2, varies between being positively and negatively correlated with Y_0.

We now describe the procedure to generate a new variable, Y_1, that has some fixed linear correlation with the existing output variable, Y_0. Assume that we have first drawn N points $\vec{x}_i$ with associated output values y_{0i}. To created a new variable with known correlation we want to mix together those y_{0i} with an uncorrelated signal, Z'. We create an uncorrelated signal by drawing N values from a unit normal distribution, z_i, performing linear least squares regression $Z = mY$, and computing an orthogonal signal $Z' = Z - mY$. Let $\sigma_{Z'}$ be the standard deviation of the residuals and let σ_{Y0} be the standard deviation of the Y_0 values. For a desired correlation coefficient ρ, the first additional output is $Y_1 = \rho \sigma_{Z'} Y_0 + \sqrt{1 - \rho^2} \sigma_{Y0} Z'$.

Because Y_0 and Z' are orthogonal, $\text{Cov}(Y_1, Y_0) = \rho \sigma_{Z'} \text{Cov}(Y_0, Y_0) = \rho \sigma_{Z'} \sigma_{Y_0}^2$. Also, $\text{Var}(Y_1) = \rho^2 \sigma_{Z'}^2 \sigma_{Y_0}^2 + (1 - \rho^2) \sigma_{Y_0}^2 \sigma_{Z'}^2 = \sigma_{Y_0}^2 \sigma_{Z'}^2$. The correlation coefficient between Y_0 and Y_1 is therefore exactly equal to ρ. In this work we set $\rho = 0.9$ unless otherwise specified.

The second additional output is defined with a quadratic equation. Let μ_{y0} be the mean of the values y_{0i}. We then define $y_{2i} = (y_{0i} - \mu_{y0})^2 + f * \mathcal{N}(0, 1)$, where f is some adjustable parameter. In this work we set $f = 0.5$ unless otherwise specified, which leads to a strong (but non-uniform) correlation.

A.3.2 Additional Output for Sequential Learning

For the purposes of synthetic sequential learning we generate the second output differently, because the intent is to create a problem in which the correlation coefficient varies depending on the region of input space. We first generate 128 inputs by sampling uniformly from the hypercube and calculate the first output y using equation 4. We then create another input, "phase," and randomly assign each point to either "A" or "B". For the points in phase A, the second output is generated using the linear procedure in the previous subsection, using $\rho = 0.98$. For the points in phase B, the second output is equal to $\sqrt{30^2 - y^2}$ (30 is the largest possible value of the Friedman-Grosse function).

This data set is plotted in Figure 3 along with dashed lines at 22 for both the first and second output, corresponding to the objectives used in the SL simulation. We see that only two points satisfy both objectives.
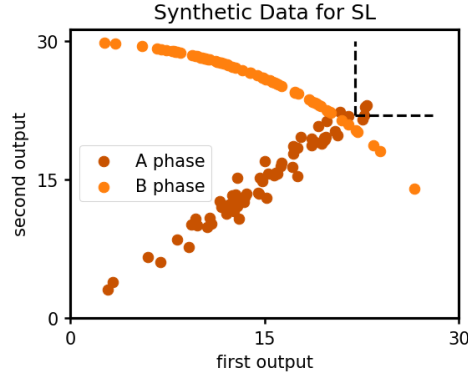
Figure 3: Synthetic data set generated using the Friedman-Grosse function for simulated sequential learning. In one region ("A phase") there is a strong positive correlation between the outputs, while in the other region ("B phase") there is a strong negative correlation between the outputs. The dashed lines correspond to the two objectives used in the simulated sequential learning study.

A.4 Friedman-Silverman

The Friedman-Silverman function [15], in Equation 5 is defined on the unit hypercube in at least 5 dimensions. In this paper we use 12 dimensions, but dimensions 6-12 do not contribute to the output.

$$y_0 = 0.1e^{4x_0} + \frac{4}{1 + e^{-20(x_1 - 0.5)}} + 3x_2 + 2x_3 + x_4 \tag{5}$$

For the purposes of investigating the predictive distribution's calibration (Figure 6), two additional outputs are generated in the same way as for the Friedman-Grosse function.

A.5 Thermoelectrics
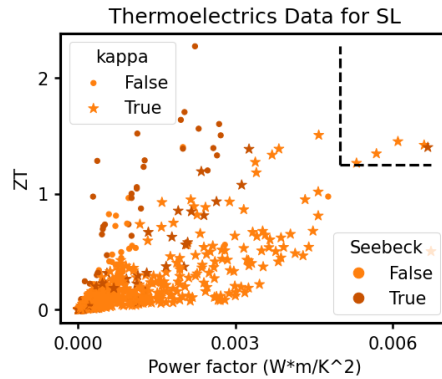
Figure 4: A projection of the thermoelectrics data set, meant to visualize the difficulty of the simulated SL problem. Dashed lines indicate the objectives for ZT (1.25) and power Factor (0.005 Wm/K^2). Points are colored red or orange according to whether or not the Seebeck coefficient exceeds the objective of 175 $\mu V/K$. The marker is a star or a circle depending on whether or not the thermal conductivity, kappa, exceeds the objective of 1.5 W/mK.

The data come from Gaultois et al. [17]. There are 688 thermoelectric materials, each with a chemical formula, crystallinity (either poly-crystalline or single crystal), and temperature at which

10
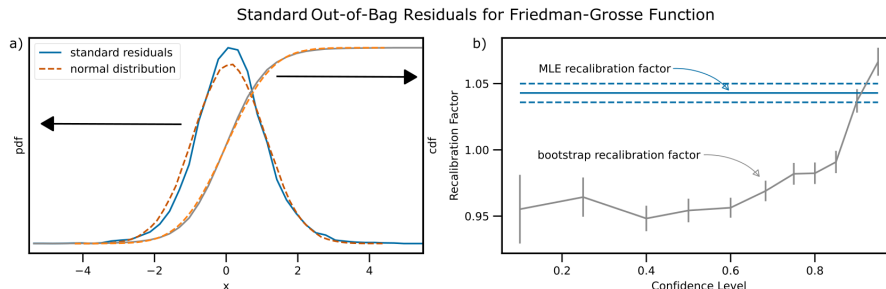
Figure 5: The standard out-of-bag (OOB) residuals approximate a normal distribution, hence the recalibrated bootstrap is expected to produce a well-calibrated prediction interval. This is seen by a) comparing the PDF and CDF to that of an ideal normal and b) checking the uniformity of the recalibration factor as a function of confidence level. We also calculate the recalibration factor generated using the MLE method and see that it is strongly influenced by outliers. Data were generated using the Friedman-Grosse function with a noise level of 2.0. There are 128 training points, 64 bags, and 100 trials.

the measurements were taken. The chemical formulae were featurized using the Matminer package [43] to calculate the Magpie features [44]. Along with temperature and crystallinity, these are the inputs to the ML models. There are five measured output properties: ZT, Seebeck coefficient, thermal conductivity, power factor, and log resistivity. One projection of this data set is plotted in Figure 4.

A.6   Mechanical Properties

The data come from Borg et al. [6]. There are 630 multi-principal element alloys, some measured under a variety of conditions. The data set contains several inputs and several outputs, many of which are sparse. To yield a dense training table we only consider the following inputs: processing method (cast, wrought, anneal, powder, and other), crystal structure (BCC, FCC, and other), test type (compression or tension), and chemical formula. The chemical formulae are featurized as with the thermoelectrics data. We only consider two output properties: Young's Modulus and Elongation.

We only keep rows that have values for all inputs and outputs. We only keep rows that were measured at room temperature (between 20 and 25°C). If there are multiple rows with identical inputs, we average their output properties. This yields 287 rows.

B   Analysis of the Recalibrated Bootstrap

B.1   Choice of Confidence Level Parameter

The choice of confidence level parameter p in algorithm 1 might seem consequential but we find in practice that it does not significantly impact the results, even when the standard residuals are noticeably not normally distributed. We investigate the impact of varying p numerically, by training a large number of random forest models on different training data draws and examining the distribution of standard OOB residuals. Results are shown in Figure 5a for the Friedman-Grosse function (see Appendix A.3). Considering both the PDF and the CDF we see that the values are evenly distributed and close to normal, but have slightly fatter tails. The inability to capture these tails is one drawback of restricting the prediction interval to be a normal distribution. The results on other test problems are similar (see Appendix E.3), though real-world data sets tend to produce a more skewed distribution. Even in those cases the normality assumption is a useful first-order approximation, as we will see in Section 5.

In Figure 5b we plot the recalibration factor vs. p. Consistent with the distribution having fat tails, we see the recalibration factor increase around $p = 0.9$ because a broader distribution is needed to capture the larger residuals. We also consider the recalibration factor that maximizes the total log likelihood of the OOB residuals, similar to what is proposed in Palmer et al. [33], and plot it as a dashed line. Maximizing the log likelihood proposes a larger recalibration factor because it is sensitive to the penalty imposed by underestimating the large residuals.

11

For the results shown in this manuscript $p = 0.683$, corresponding to one standard deviation. A larger value of p would produce prediction intervals that are slightly wider. Exactly how this impacts sequential learning depends on the acquisition function, and is a potential topic for further study. In section E.5 we compare the results of simulated SL using both $p = 0.683$ and $p = 0.95$ (corresponding to two standard deviations) and find that there is no statistical difference.

B.2 Random Forest as a Weighted Combination of Training Data

A random forest model can be considered a piece-wise local weighted combination of the training. This framing, described below, will be useful in the subsequent sections.

A decision tree partitions the domain into rectangular subspaces, each corresponding to a terminal node of the tree. The prediction in this subspace is the average of the values of the training data that appear in that node. This training data $\rightarrow$ subspace correspondence is a complicated function of the training data, the splitting function, and random variables (such as which input dimensions are being considered), but we can write the tree's predictions as a weighted sum of the training data. The RF prediction is therefore given by equation 6, where $\{Z_n\} \in Z$ is represents the training data draw of size n and $\phi \in \Phi$ represents a random variables that controls the splitting. The weights $w_{bi}(\vec{x})$ are non-zero only when $\vec{x}_i$ is "close" to $\vec{x}$, and the weights sum to 1 for each tree and value of $\vec{x}$.

$$\hat{\theta}(\vec{x}) = \frac{1}{B} \sum_{b=1}^{B} \sum_{i=1}^{N} w_{bi}(\vec{x}; \{Z_n\}, \phi) y_i \tag{6}$$

The out-of-bag prediction for $\vec{x}_i$ is similar, but the sum is taken only over the trees for which $\vec{x}_i$ is not present in the bootstrap sample. This is, on average, B/e trees.

$$\hat{\theta}_{(-i)}(\vec{x}_i) = \frac{1}{B/e} \sum_{b:z_i \notin Z_b} \sum_{j} w_{bj}(\vec{x}_i; \{Z_n\}, \phi) y_i \tag{7}$$

B.3 Asymptotic Equivalence of Standard Residual Distributions

We wish to show that the distribution of true standard residuals is equivalent to the distribution of OOB standard residuals:

$$\left\langle \frac{\hat{\theta}_{(-i)}(\vec{x}_i) - y_i}{\hat{s}_{(-i)}(\vec{x}_i)} \right\rangle_{\{Z_n\}, \phi, z_j} \stackrel{?}{=} \left\langle \frac{\hat{\theta}(\vec{x}) - (f(\vec{x}) + \epsilon \mathcal{N}(0,1))}{\hat{s}(\vec{x})} \right\rangle_{\{Z_n\}, \phi, x, y} \tag{8}$$

The expectation is taken over all training data draws $\{Z_n\}$ and parameters ϕ, and on the LHS over all training data $(\vec{x}_j, y_j) \in \{Z_n \backslash z_i\}$ while on the RHS it is over all $\vec{x}$ in the domain and all associated observations drawn from $y = f(\vec{s}) + \epsilon \mathcal{N}(0, 1)$.

Consider what a fixed point $\vec{x}$ contributes to each side of this equation. Because the labels y_i are generated according to $f(\vec{x}) + \epsilon \mathcal{N}(0, 1)$, and drawing the noise at $\vec{x}$ is independent of $\hat{s}(\vec{x})$, we can replace both y_i and $f(\vec{x}) + \epsilon \mathcal{N}(0, 1)$ in expectation with $f(\vec{x})$. On the LHS we therefore have the mean standard residual at $\vec{x}$ for an RF model trained with $N - 1$ iid training points and B/e trees. On the right we have the mean standard residual at $\vec{x}$ for an RF model trained with N iid training points and B trees. For large values of B and N, these are equivalent.

B.4 Bootstrap Variance is Sensitive to the True Error

The total expected squared error due to a model can be represented as the sum of the bias squared, the model variance, and the noise variance. We wish to show that the bootstrap variance (and hence the recalibrated bootstrap standard deviation) is sensitive to each of these terms.

B.4.1 Noise Variance

The bootstrap variance is written in Equation 9

$$\langle \hat{s}^2(\vec{x})\rangle = \left\langle \frac{1}{B-1}\sum_b (t_b(\vec{x}) - \hat{\theta}(\vec{x}))^2 \right\rangle_{\{Z_n\},\phi} = \frac{B}{B-1}\langle t_b(\vec{x})^2\rangle_{\{Z_n\},\phi,b} - \frac{B}{B-1}\langle \hat{\theta}(\vec{x})^2\rangle_{\{Z_n\},\phi}$$

$$(9)$$

The simplification is possible because $\hat{\theta}$ is the mean of t_b. First, we consider the expectation of $t_b(\vec{x})^2$:

$$\langle t_b(\vec{x})^2\rangle_{\{Z_n\},\phi,b} = \left\langle \left(\sum_i w_{bi}(\vec{x}; \{Z_n\}, \phi)(f(\vec{x}_i) + \epsilon\mathcal{N}(0,1)) \right)^2 \right\rangle_{\{Z_n\},\phi,b} \qquad (10)$$

The weights $w_{bi}(\vec{x})$ mostly depend on which training data are "close" to $\vec{x}$ in input space. There is some dependence on the exact values of y_i, but we can consider the weights w_{bi} to be roughly independent of the noise drawn from $\epsilon\mathcal{N}(0,1)$. In that case the expectation simplifies to Equation 11, where L is the typical number of unique training observations on a leaf node.

$$\langle t_b(\vec{x})^2\rangle \approx \left\langle \left(\sum_i w_{bi}(\vec{x}; \{Z_n\}, \phi)f(\vec{x}_i) \right)^2 \right\rangle_{\{Z_n\},\phi,b} + \frac{\epsilon^2}{L} \qquad (11)$$

Similarly, $\langle \hat{\theta}(\vec{x})^2\rangle_{\{Z_n\},\phi}$ also has a term that goes as ϵ^2. But since there is an additional average over the bootstrap samples and each bootstrap sample masks off some training data, there will be a larger number of independent noise draws being averaged together and hence the effective value of L is larger. Therefore, $\langle \hat{s}(\vec{x})^2\rangle$ has a term that is proportional to the noise variance ϵ^2. This term is smaller if there are more training examples on each leaf node, but that makes sense since we would expect a model that averages over more training data to be less sensitive to the noise.

In Appendix D we show that, as the noise becomes the dominant term, the recalibrated bootstrap correctly identifies each observation as being an independent random variable with uncertainty equal to the noise.

B.4.2 Model Variance

Having considered the noise, we set $\epsilon = 0$ for the remainder of this Appendix. We next consider the variance due to the finite training data set size and the parameters of the model, $\langle \hat{\theta}(\vec{x})^2\rangle_{\{Z_n\},\phi} - \langle \hat{\theta}(\vec{x})\rangle^2_{\{Z_n\},\phi}$. Assume for now that there is no bias, so $\langle \hat{\theta}(\vec{x})\rangle = f(\vec{x})$, and without loss of generality assume $f(\vec{x}) = 0$. Our task is to show that $\langle \hat{s}(\vec{x})^2\rangle \propto \langle \hat{\theta}(\vec{x})^2\rangle_{\{Z_n\},\phi}$, which by Equation 9 is equivalent to showing that $\langle t_b(\vec{x})^2\rangle_{\{Z_n\},\phi,b} \propto \langle \hat{\theta}(\vec{x})^2\rangle_{\{Z_n\},\phi}$.

But this is clearly true because $\hat{\theta}(\vec{x})$ is the mean of $t_b(\vec{x})$. Consider some fixed $\{Z_n\}$ and ϕ. The $t_b(\vec{x})$ are the predictions made by all trees trained on bootstrap replicates of $\{Z_n\}$. The $\hat{\theta}(\vec{x})$ are the averages of all sets of B draws from the distribution of $t_b(\vec{x})$. By the law of large numbers, the variance of the latter is equal to the variance of the former times $1/B$. Hence, $\langle \hat{s}(\vec{x})^2\rangle$ is sensitive to model variance.

B.4.3 Bias Squared

Assume for simplicity that the training data are independent and identically distributed, that $f(\vec{x})$ is continuous, and that the random forest is full-depth. In this case the model is asymptotically consistent and free of bias *except* for at the boundaries. As a way of illustrating how the bootstrap variance can pick up bias, we consider the boundary of a one-dimensional test problem. A more rigorous investigation would need to consider multivariate and non-identically distributed data, which is the case for the real-world data sets used here.

Let the domain be $[0,1]$ and let the function $f(x)$ have slope m at $x = 0$. Because the trees are grown to full depth the predicted value at $x = 0$ will be equal to the value of the training point with the smallest value of x. Because the training data are drawn uniformly this is equal in expectation to $1/(N+1)$. Assuming the linear approximation of $f(x)$ is valid over the length-scale of $1/(N+1)$, the predicted value will therefore be equal in expectation to $m/(N+1)$.

However, roughly $1/e$ trees will be missing this data point. Most of these trees will make a prediction that is equal to the value of the training point with the second-smallest value of x, which in expectation is at $2/(N+1)$ and has a value of $2m/(N+1)$. There are other terms as well, but they are all proportional to $m/(N+1)$. Hence the bias goes as $m/(N+1)$ and the bias squared goes as $m^2/(N+1)^2$.

Now consider the bootstrap variance, which is the mean of $(t_b(0) - \hat{\theta}(0))^2$. As discussed above, $t_b(0)$ is always proportional to $m/(N+1)$. Hence $\hat{\theta}(0) \propto m/(N+1)$. Though the sum is complex, every term has a factor of $m/(N+1)$ that can be factored out, and so the bootstrap variance goes as $m^2/(N+1)^2$, just like the bias squared does.

B.4.4 Conclusion

These arguments are not precise, and in fact we do not expect the bootstrap variance to perfectly capture the true residual. We merely show that it has the capability to pick up on the bias, the variance, and the noise. Its efficacy and ability to balance these three terms is shown through the numerical experiments in this manuscript.

C More Details on Numerical Experiments

Unless otherwise stated all random forests contained 64 decision trees. All decision trees were grown to full depth and all inputs were considered at each split. The split was chosen to maximize the reduction in total variance summed over all outputs. All outputs were standardized before training to have mean 0 and variance 1. Unless otherwise stated the recalibration factor is $p = 0.683$, corresponding to $\eta \approx 1$.

C.1 Metrics

We consider three metrics of prediction interval quality.

Standard Error: the mean of the absolute residual divided by the predicted uncertainty, as given in Equation 12 (the sum is over the test data). This value should be around 1.0, and it should be stable as the number of training data are varied. This metric is only used for univariate prediction intervals.

$$\texttt{Standard Error} = \frac{1}{M} \sum_j \frac{|\hat{\theta}(\vec{x}_j) - y_j|}{\hat{\sigma}(\vec{x}_j)} \tag{12}$$

Standard Confidence: how closely does the number of residuals within some magnitude match the number of residuals that are *expected* to be within that magnitude? The magnitude of the residual is the Mahalanobis distance, $r_M = \sqrt{\vec{r}^T \hat{\Sigma}(\vec{x}_j)^{-1} \vec{r}}$, where $\vec{r} = \hat{\vec{\theta}}(\vec{x}_j) - \vec{y}_j$ is the residual. The squared Mahalanobis distance follows a χ^2 distribution with d degrees of freedom, where d is the number of output dimensions. For a given coverage level $p_c \in (0, 1)$ we can therefore use the inverse CDF of χ_d^2 to calculate the associated cutoff distance η_c, and count the number of observations for which $r_M < \eta_c$. In one dimension this reduces to Equation 13

$$\texttt{Standard Confidence} = \frac{1}{M} \sum_j \mathbb{1}\left[\frac{|\hat{\theta}(\vec{x}_j) - y_j|}{\hat{\sigma}(\vec{x}_j)} \leq \Phi^{-1}\left(\frac{1+p_c}{2}\right) \right] \tag{13}$$

If the standard confidence is greater than p_c then the model is under-confident, and if it is less than p_c then the model is over-confident. In this work we use "standard confidence" to refer to the case when $p_c \approx 0.683$.

Median Negative Log Probability Density (MNLPD): Let $p(\vec{y}; \hat{\vec{\theta}}(\vec{x}), \hat{\Sigma}(\vec{x}))$ be the probability density function of the predictive distribution at point $\vec{x}$. The NLPD for test point $(\vec{x}_j, \vec{y}_j)$ is given by Equation 14. Lower values are better. NLPD penalizes both over- and under-confident prediction intervals. Because NLPD is prone to outliers (especially for the jackknife method), here we consider the median value over all test points.

$$\text{NLPD}(\vec{x}_j) = -\ln(p(\vec{y}_j; \hat{\vec{\theta}}(\vec{x}_j), \hat{\Sigma}(\vec{x}_j))) \tag{14}$$

C.2 Alternative Methods of Calculating the Correlation Coefficient

We consider the following methods of calculating $\hat{\rho}_{jk}(\vec{x})$.

1. **Trivial**: $\hat{\rho}_{jk} = 0$, the probability of satisfying each objective is considered independently. In the absence of existing methods to compute multivariate prediction intervals, this is the baseline approach.

2. **Training Data**: Calculate the Pearson correlation coefficient over the training data and and use that value for all predictions.

3. **Jackknife**: Calculate the jackknife variance, V_J, and the jackknife covariance, Cov_J, and set $\hat{\rho}_{jk} = \text{Cov}_J[j,k]/\sqrt{V_J[j] * V_J[k]}$. See Appendix D for more details.

4. **Bootstrap**: Calculate the Perason correlation coefficient over the tree-wise predictions as in Equation 2. This is the approach we are proposing here.

It might seem strange to consider the jackknife method, since it produces a quantity that is known to be more confident than a prediction interval. But it is possible that this bias will cancel out between the variance and covariance terms, leaving us with a decent estimate of correlation.

C.3 Multivariate Calibration Results
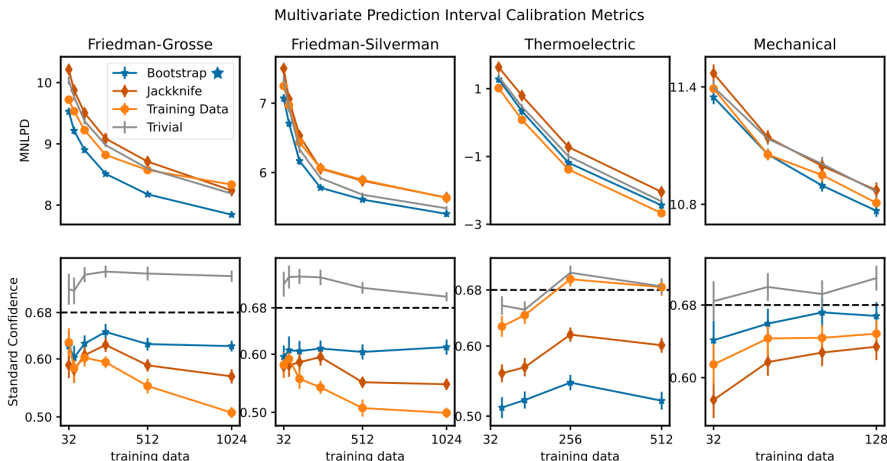
Figure 6: The recalibrated bootstrap produces the best overall multivariate prediction intervals on a suite of test problems, as judged by a low MNLPD (top row) and a standard confidence that is close to 0.68 (bottom row). Error bars show one standard error. The four test problems are Friedman-Grosse with noise 2.0 (128 test points, 16 trials), Friedman-Silverman with noise 2.0 (128 test points, 16 trials), thermoelectrics (64 test points, 32 trials), and mechanical properties (48 test points, 32 trials). See Appendix A for details.

C.4 Details of Simulated Sequential Learning

Sequential learning may be done with any multi-objective acquisition function. Here we use the predicted probability of the candidate lying in the satisfactory region, estimated by drawing 10,000 samples from the predictive distribution. In other situations it might be preferable to use other acquisition functions, such as the probability of being Pareto non-dominated [9].

We simulate SL on two problems. First, we modify the Friedman-Grosse function to generate two outputs that have a non-trivial relationship to each other. The outputs are positively correlated in one region and negatively correlated in another region. See Appendix A.3 for more details. The

objectives are that each output should exceed 22, a value chosen to make the problem challenging. As seen in Figure 3 of Appendix A.3, only two points satisfy both objectives. Each trial starts with 16 randomly-selected training data.

Second, we consider the thermoelectrics data set and devise a problem for which there is one solution: ZT > 1.25, Seebeck coefficient > 175 μV/K, power factor $> 5 \times 10^{-3}$ Wm/K^2, and thermal conductivity > 1.5 W/mK. The data are plotted in Figure 4 of Appendix A.5. Each trial starts with 32 randomly-selected training data.

C.5   Results of Simulated Sequential Learning

These are the results shown in Figure 2. In addition to the four methods of calculating the correlation coefficient we also consider the distribution that would occur if the candidates were selected at random.

Table 1: Distribution of rounds required to find a satisfactory candidate in simulated sequential learning. Mean values are reported along with one standard error. Results are calculated over 64 independent trials.

	Method	mean	5th percentile	median	95th percentile
Synthetic Data (2 objectives)	Trivial	36.0 ± 2.6	2	43	61
	Training Data	41.8 ± 3.1	2	51	72
	Jackknife	11.2 ± 1.5	**1**	7	37.7
	Bootstrap	**7.5 ± 1.0**	**1**	**4.5**	**22.7**
	Random	36	3	33	87
Thermoelectrics Data (4 objectives)	Trivial	330 ± 25	15	309	630
	Training Data	230 ± 19	19	200.5	532.5
	Jackknife	240 ± 21	35	203	568
	Bootstrap	**170 ± 20**	**8**	**125**	**497**
	Random	328	33	328	623

D   Details of Jackknife Variance and Covariance (Including the Bias-Correction Term)

Wager et al. [40] introduces bias-corrected versions of two methods to estimate a confidence interval: the Infinitesimal Jackknife (IJ) and the Jackknife after Bootstrap (JaB). Here we generalize those derivations from variance to covariance. Wager et al. [40] found that the IJ and JaB had opposite lowest-order biases, and hence suggested averaging them. In this manuscript, whenever "jackknife methods" are invoked, it is the average of the IJ and the JaB (co)variance. The square root of this term is referred to as the "jackknife standard deviation."

Although the derivations below consider covariance between two outputs predicted by one ensemble model at one input point, they also apply to the covariance between predictions made at two distinct input points or to predictions made by two distinct ensemble models. Indeed, Ghosal [18] derive an analogue of Equation 15 but their focus is on the covariance between the predictions made by two models, in order to test if the models are equivalent.

D.1   Infinitesimal Jackknife Covariance

We show that the bias-corrected IJ covariance between outputs j and k at point $\vec{x}$ is given by Equation 15, where Y_{bi} is the number of times training datum i appears in bag b.

$$\text{Cov}_{IJ}[j,k](\vec{x}) \approx \sum_{i=1}^{N} \left(\sum_{b=1}^{B} \frac{(Y_{bi} - 1)(t_{bj}(\vec{x}) - \hat{\theta}_j(\vec{x}))}{B} \right) \left(\sum_{b=1}^{B} \frac{(Y_{bi} - 1)(t_{bk}(\vec{x}) - \hat{\theta}_k(\vec{x}))}{B} \right)$$

$$- \frac{N-1}{B} \sum_{b=1}^{B} (t_{bj}(\vec{x}) - \hat{\theta}_j(\vec{x}))(t_{bk}(\vec{x}) - \hat{\theta}_k(\vec{x})) \tag{15}$$

D.1.1 Main Term

We follow the arguments in Efron [12], which themselves are similar to those in Efron [11], but we generalize to covariance. Consider two estimators, $\hat{\theta}_j$ and $\hat{\theta}_k$, that evaluate some functions θ_j and θ_k for a given distribution of training data. For our purposes, θ_j and θ_k correspond to two outputs that the model predicts. The predictions depend on the bootstrap samples, which are generated by drawing N samples from N training data according to some probability vector, $\vec{p}$ of length N. For an ordinary bootstrap, $\vec{p} = \vec{p}_0$, a uniform vector for which each entry is equal to $1/N$. Equivalently, this can be thought of as an isotropic rescaled multinomial distribution, $\mathbb{M}$.

We are therefore interested in the covariance between $\theta_j(\vec{p})$ and $\theta_j(\vec{p})$ over the multinomial distribution. Both θ_j and θ_k are effectively functions of $\vec{p}$, and we linearize them around $\vec{p}_0$ as $\theta_j(\vec{p}) = \theta_j(\vec{p}_0) + (\vec{p} - \vec{p}_0) \cdot \vec{U}$, where $\vec{U}$ is the influence function. Similarly, let $\vec{V}$ be the influence function of $\theta_j(\vec{p})|_{\vec{p}_0}$. Because $\sum_i U_i = \sum_i V_i = 0$, the covariance reduces as shown below.

$$\begin{aligned}
\text{Cov}_{\mathbb{M}}[\theta(\vec{p}), \phi(\vec{p})] &= \mathbb{E}_{\mathbb{M}}[(\theta(\vec{p}) - \bar{\theta}(\vec{p}))(\phi(\vec{p}) - \bar{\phi}(\vec{p}))] \\
&= \mathbb{E}_{\mathbb{M}}[(\vec{p} - \vec{p}_0) \cdot \vec{U}(\vec{p} - \vec{p}_0) \cdot \vec{V})] \\
&= \mathbb{E}_{\mathbb{M}}[(\vec{p} \cdot \vec{U})(\vec{p} \cdot \vec{V})] \\
&= \mathbb{E}_{\mathbb{M}} \left[\sum_{i=1}^{N} p_i^2 U_i V_i + \sum_{i=1}^{N} \sum_{l \neq i} p_i p_l U_i V_l \right. \\
&= \sum_{i=1}^{N} U_i V_i \mathbb{E}_{\mathbb{M}}[p_i^2] + \sum_{i=1}^{N} \sum_{l \neq i} U_i V_l \mathbb{E}_{\mathbb{M}}[p_i p_l]
\end{aligned}$$

The expectation values of p_i^2 and $p_i p_j$ are those of $\mathbb{M}$, for which the mean of each term is $1/N$, the variance of each term is $1/N^2 - 1/N^3$, and the covariance between any pair of terms is $-1/N^3$. This yields the following.

$$\text{Cov}_{\mathbb{M}}[\theta_j(\vec{p}), \theta_k(\vec{p})] = \frac{1}{N^2} \sum_{i=1}^{N} U_i V_i$$

What are U_i and V_i? By taking the derivative, Efron [12] derives them to be equal to $N\text{Cov}_*[Y_{bi}, t_b(\vec{x})]$. The asterisk indicates that the covariance is taken over the bootstrap samples. The IJ covariance estimate between outputs j and k is therefore given by Equation 16, which is a natural generalization of the IJ variance.

$$\text{Cov}_{IJ}[j,k](\vec{x}) = \sum_{i=1}^{N} \text{Cov}_*[Y_{bi}, t_{bj}(\vec{x})] \text{Cov}_*[Y_{bi}, t_{bk}(\vec{x})] \tag{16}$$

When expanding this covariance explicitly we need to know the mean values of Y_{bi} and t_b, which are 1 and $\hat{\theta}$.

D.1.2 Bias Correction Term

Equation 16 is exact as $B \to \infty$, but in practice we only consider a subset of bags. Let $A_j^B = \text{Cov}_*[Y_{bi}, t_{bj}(\vec{x})]$ and A_j^∞ be the same for infinite B. One term of the IJ sum is, in expectation:

$$\mathbb{E}_*[A_j^B A_k^B] = \mathbb{E}_*[A_j^B]\mathbb{E}_*[A_k^B] + \text{Cov}_*[A_j^B, A_k^B]$$
$$= A_j^\infty A_k^\infty + \text{Cov}[A_j^B, A_k^B]$$

The difference between the finite-B value and the ideal value is therefore given by $-N\text{Cov}_*[A_j^B, A_k^B]$. Writing this out in detail we get Expression 17, where the expectation is now taken over the training data.

$$-\frac{N}{B}\mathbb{E}\Big[\text{Cov}_*[Y_{bi} * (t_{bj}(\vec{x})) - \hat{\theta}_j(\vec{x}), Y_{bi} * (t_{bk}(\vec{x}) - \hat{\theta}_j(\vec{x}))]\Big] \tag{17}$$

As in Wager et al. [40] we treat Y_{bi} and t_b as independent, meaning we can pull out the Y_{bi} terms into their own variance term $\text{V}_*[Y_{bi}]$, which is equal to the variance of a multinomial distribution, or $(N-1)/N$. The remaining covariance between the trees t_{bj} and t_{bk} is written out explicitly, and we arrive at the following bias-correction term.

$$-\frac{N-1}{B}\sum_{b=1}^{B}(t_{bj}(\vec{x}) - \hat{\theta}_j(\vec{x}))(t_{bk}(\vec{x}) - \hat{\theta}_k(\vec{x})) \tag{18}$$

Note that this differs slightly from the bias-correction in Wager et al. [40], because they mistakenly set the variance of Y_{bi} equal to 1 and hence have a factor of N instead of $N-1$ (this occurs right before equation 11 in Wager et al. [40]).

Combining Equations 16 and 18 we arrive at Equation 15

D.2 Jackknife after Bootstrap Covariance

We show that the bias-corrected JaB covariance between outputs j and k at point $\vec{x}$ is given by Equation 19.

$$\text{Cov}_{JaB}[j,k](\vec{x}) \approx \frac{N-1}{N}\sum_{i=1}^{N}\Big(\hat{\theta}_{j(-i)}(\vec{x}) - \hat{\theta}_j(\vec{x})\Big)\Big(\hat{\theta}_{k(-i)}(\vec{x}) - \hat{\theta}_k(\vec{x})\Big)$$
$$- (e-1)\frac{N-1}{B}\sum_{b=1}^{B}(t_{bj}(\vec{x}) - \hat{\theta}_j(\vec{x}))(t_{bk}(\vec{x}) - \hat{\theta}_k(\vec{x})) \tag{19}$$

D.2.1 Main Term

The derivation of the JaB in Efron [11] is identical to that of the IJ, but the influence function is different. The generalization to covariance therefore works out the same way and we get Equation 20.

$$\text{Cov}_{JaB}[j,k](\vec{x}) = \frac{N-1}{N}\sum_{i=1}^{N}\Big(\hat{\theta}_{j(-i)}(\vec{x}) - \hat{\theta}_j(\vec{x})\Big)\Big(\hat{\theta}_{k(-i)}(\vec{x}) - \hat{\theta}_k(\vec{x})\Big) \tag{20}$$

D.2.2 Bias Correction Term

The derivation of the JaB bias term is the same as it is for the IJ, above, but instead of A_j^B the relevant term for some training datum i is now $\hat{\Delta}_{ij} \equiv \hat{\theta}_j^B - \hat{\theta}_{(-i)j}^B$ (the dependence on $\vec{x}$ is elided for simplicity) and there is also an overall factor of $(N-1)/N$. In order to evaluate $\text{Cov}_*[\hat{\Delta}_{ij}, \hat{\Delta}_{ij}]$ we follow Appendix A of Wager et al. [40] but generalize from variance to covariance.

Using the law of total covariance, we can expand this term out as follows:

$$\text{Cov}_*[\hat{\Delta}_{ij}, \hat{\Delta}_{ik}] = \mathbb{E}_*\Big[\text{Cov}_*[\hat{\Delta}_{ij}|B_i, \hat{\Delta}_{ik}|B_i]\Big] + \text{Cov}_*\Big[\mathbb{E}_*[\hat{\Delta}_{ij}|B_i], \mathbb{E}_*[\hat{\Delta}_{ik}|B_i]\Big]$$

The "covariance of expectation" term simplifies just as the analogous "variance of expectation" term in Wager et al. [40], to $\Delta_{ij}\Delta_{ik}\mathcal{O}(1/B)$, where the Δ terms without a hat indicate the average over all possible bootstrap samples.

To evaluate the "expectation of covariance" term we re-write $\hat{\Delta}$ as a sum over B_i bags that do not contain point i and a subsequent sum over $B - B_i$ bags that do contain point i. On average, $B_i = B/e$.

$$\hat{\Delta}_{ij} = \frac{1}{B_i}\sum_{b=1}^{B_i} t_{bj} - \frac{1}{B}\sum_{b=1}^{B} t_{bj} = \frac{B - B_i}{BB_i}\sum_{b=1}^{B_i} t_{bj} - \frac{1}{B}\sum_{b=B_i+1}^{B} t_{bj}$$

The covariance between $\hat{\Delta}_{ij}$ and $\hat{\Delta}_{ik}$ then breaks out into the sum of many covariance terms, all of the form $\text{Cov}[t_{bj}, t_{b'k}]$. But because the bags are independent, all of these terms are 0 unless $b = b'$. We therefore have B_i instances of $\text{Cov}[t_{bj}|B_i = 0, t_{bk}|B_i = 0]$ and $B - B_i$ instances of $\text{Cov}[t_{bj}|B_i \neq 0, t_{bk}|B_i \neq 0]$, which we denote $cov_i^{(0)}$ and $cov_i^{(+)}$.

$$\text{Cov}_*[\hat{\Delta}_{ij}|B_i, \hat{\Delta}_{ik}|B_i] = \left(\frac{B - B_i}{BB_i}\right)^2 B_i cov_i^{(0)} + \frac{1}{B^2}(B - B_i)cov_i^{(+)} \tag{21}$$

Equation 21 is identical to the analogous equation in Wager et al. [40] except that we have the covariance between t_{bj} and t_{bk} instead of the variance of t_b. Calculating the expectation therefore proceeds the same way and we wind up with, to lowest order, $\frac{e-1}{B}\text{Cov}_*[t_{bj}, t_{bk}]$. Including the factor of $(N - 1)/N$ and the sum over N, we wind up with expression 22.

$$-(e-1)\frac{N-1}{B}\sum_{b=1}^{B}(t_{bj}(\vec{x}) - \hat{\theta}_j(\vec{x}))(t_{bk}(\vec{x}) - \hat{\theta}_k(\vec{x})) \tag{22}$$

Note that this is again slightly different from Wager et al. [40], who convert the factor of $N - 1$ into a factor of N for unclear reasons.

Combining Equations 20 and 22 we arrive at Equation 19.

E More Numerical Experiments

E.1 The Jackknife Underestimates the True Model Error

We consider two one-dimensional test problems, a double tophat and a cubic on the domain [-1, 1] (see Appendix A for details). We draw 64 training data uniformly, train an RF model, and calculate its predictions on 100 points evenly spaced throughout the domain. We also calculate the jackknife standard deviation (see Appendix D) and the squared error at these points. This is averaged over 250 trials. The results, in Figure 7, show that a jackknife-based prediction interval can be highly over-confident, in particular when the model is biased.

E.2 Performance on Imbalanced Data

Table 2 shows univariate uncertainty metrics when the training and test sets are drawn from highly imbalanced distributions. We use the Young's Modulus output of the Mechanical Properties data set. In these data there are points that were measured under tension and points that were measured under compression. The training set consists of 60 tension points and 4 compression points. The test set consists of 32 compression points. We calculate prediction interval metrics for both the recalibrated bootstrap method and the method of Zhang et al. [45], which uses the out-of-bag residuals to compute an unconditional prediction interval. We refer to this method as "OOB constant." 50 trials were run, each involving a different draw of training/test data. Models were trained with 64 bags. Error bars are one standard error.

We see that the OOB constant method is highly over-confident – the true residual is on average more than twice as large as the 1-σ error bar. The recalibrated bootstrap is also over-confident
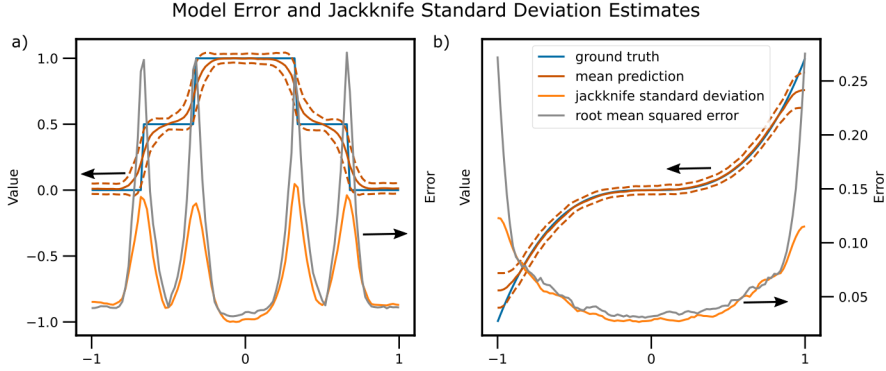
Figure 7: Jackknife standard deviation and true model root mean squared error (RMSE) for two one dimensional test functions: a) tophat and b) cubic. The ground truth and predicted value (with ± 1 standard deviation) are plotted on the left axis. The jackknife standard deviation and the RMSE are both plotted on the right axis.

but significantly less so. Interestingly the MNLPD values are equivalent, highlighting the fact that MNLPD must be considered as one of several metrics. The recalibration method of Palmer et al. [33] essentially minimizes NLPD, and hence may also have trouble with imbalanced data.

Table 2: Comparison of the "recalibrated bootstrap" and "empirical OOB residuals" Zhang et al. [45] prediction interval methods on a problem for which the training and test sets are drawn from different distributions.

	MNLPD	Standard RMSE	Standard Confidence
Empirical OOB Residuals	7.37 ± 0.06	2.12 ± 0.07	0.38 ± 0.02
Recalibrated Bootstrap	7.39 ± 0.02	$\mathbf{1.35 \pm 0.07}$	$\mathbf{0.61 \pm 0.03}$

E.3 Recalibration Factors

Figure 8 shows the distribution of standard residuals and recalibration factors (as in Figure 5) for four more test problems: Friedman-Grosse without noise, Friedman-Silverman, the Elongation output of the Mechanical Properties data set, and the ZT output of the Thermoelectrics data set.

We see that the other synthetic problems are well calibrated but also have some high-residual outliers. The real-world data sets are skewed and more sharply peaked.

E.4 Prediction Interval Metrics

Figure 9 shows the univariate prediction interval metrics (as in Figure 1 for four more test problems: Friedman-Grosse without noise, Friedman-Silverman with noise of magnitude 2.0, the Young's Modulus output of the mechanical properties data set, and the ZT output of the thermoelectrics data set.

Figure 10 shows MNLPD for the multivariate Friedman-Grosse test problem with 128 test and training points, varying the number of bags. The number of bags is largely irrelevant. The fact that a small, constant number of bags suffices to create a well-calibrated prediction interval is one of the benefits of the recalibrated bootstrap method.

Figure 11 shows the effect of varying the noise level for the Friedman-Grosse test problem. For a single output we consider the size of the mean 1-σ prediction interval generated by the recalibrated bootstrap, divided by the noise level. Ideally this would approach 1 as the noise becomes dominant. Instead it approaches 1.1. The standard residual (not shown) approaches 0.9, so we see that while the recalibrated bootstrap largely picks up on the noise it is not quantitatively exactly correct.

For the multi-output problem we see that the recalibrated bootstrap and trivial methods of estimating correlation converge to the same result in the high-noise limit. Since the noise is generated independently, the correlation coefficients of the predictive distribution should be uniformly 0 in this limit. The trivial method is therefore correct, and the fact that the recalibrated bootstrap method converges to the same result indicates that it is hitting upon this correct answer as well.

E.5 Impact of Confidence Level Parameter on Sequential Learning

Table 3 shows the impact of varying the confidence level parameter in the recalibrated bootstrap algorithm. Changing the value of p can change the recalibration factor and lead to a slight uniform rescaling of the prediction intervals. For the synthetic problem based on the Friedman-Grosse function (Appendix A.3), we know from Figure 5b that setting $p = 0.95$ generally leads to a larger recalibration ratio and wider prediction intervals. However this is not seen to impact the results of simulated SL.

Table 3: Mean number of iterations required to find a satisfactory candidate in the synthetic sequential learning problem, comparing two values of the confidence level parameter from Algorithm 1. Uncertainty values are one standard error computed over 64 independent trials.

	$p = 0.683$ (1-σ)	$p = 0.95$ (2-σ)
Trivial	36.0 ± 2.6	35.1 ± 2.8
Training Data	41.8 ± 3.1	41.7 ± 2.9
Jackknife	11.2 ± 1.5	11.9 ± 1.6
Bootstrap	7.5 ± 1.0	7.5 ± 1.0
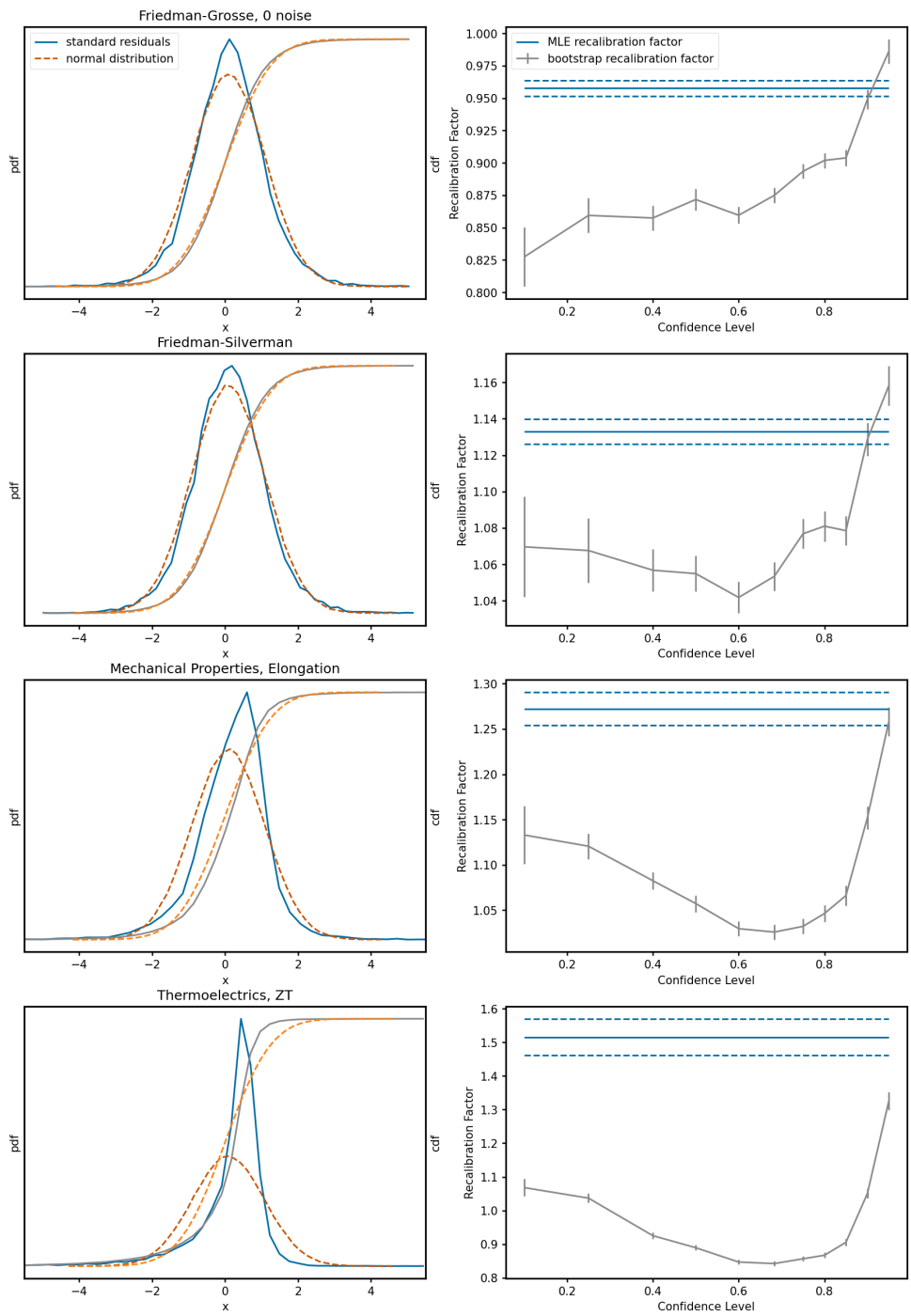
Figure 8: Investigation of the standard OOB residuals and recalibration factors for several test problems.
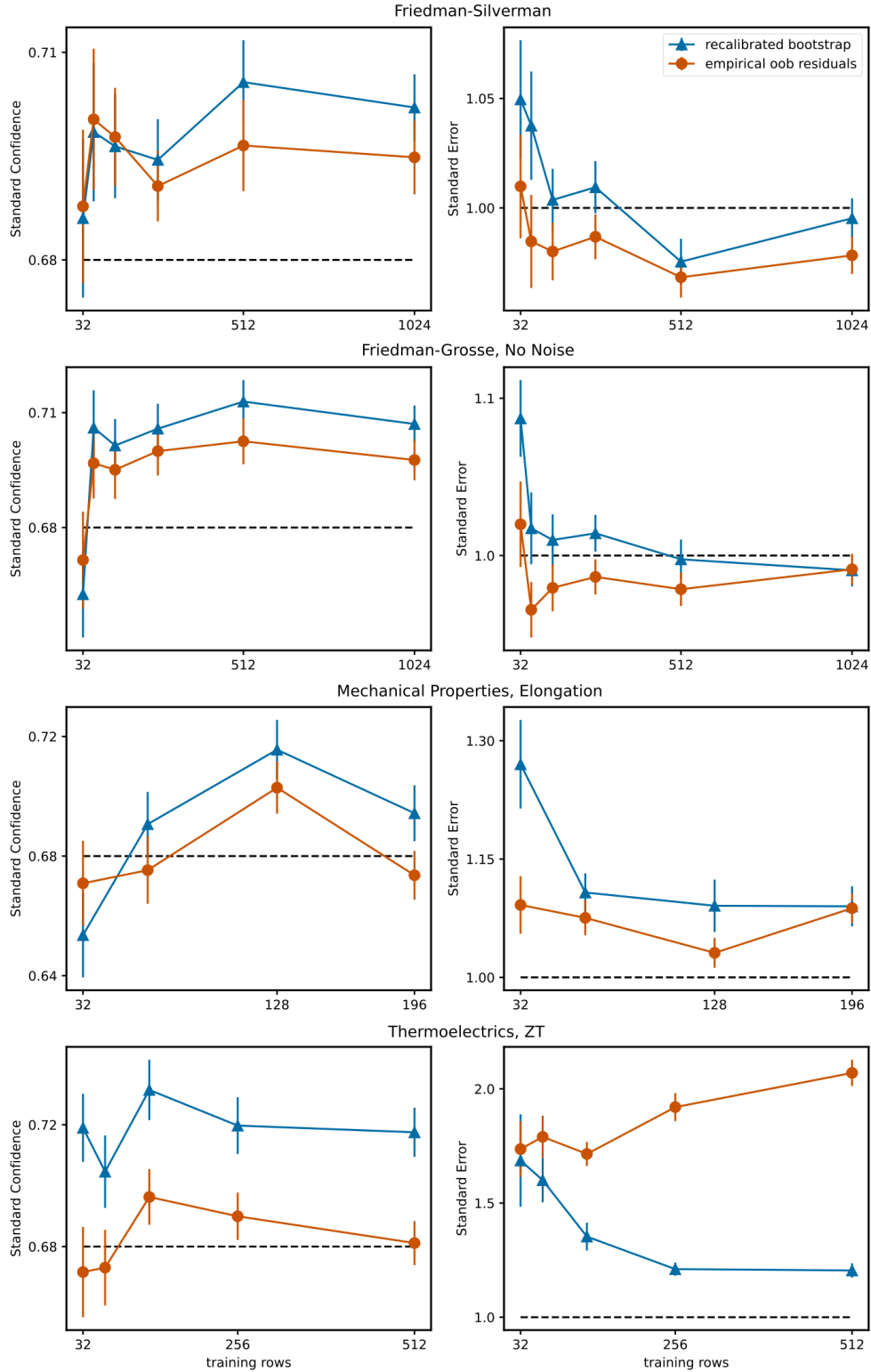
Figure 9: Univariate prediction interval metrics for several test problems, computed using the recalibrated bootstrap method proposed here and the "empirical OOB residuals" method of Zhang et al. [45]. Synthetic problem have 128 test points; real data test problems have 64 test points. All results are averaged over 64 trials. Each trial involves a different set of training and test data. Error bars are 1 standard error.
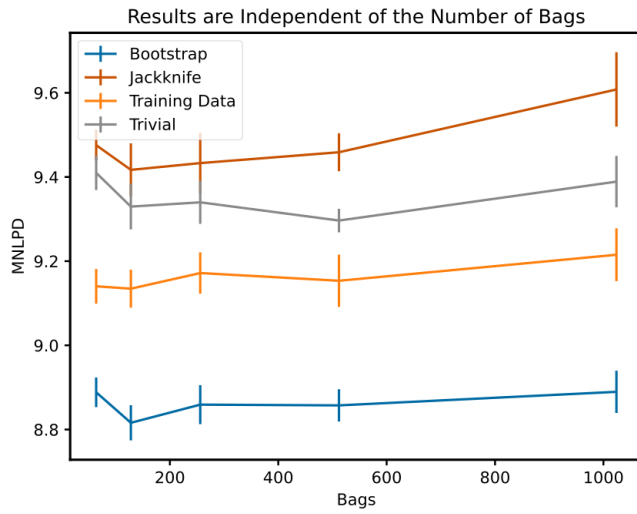
Figure 10: Increasing the number of bags does not change the relative accuracy of the correlation estimation methods. This test is on the Friedman-Grosse function with noise level 1.0, 128 training and test points, and 16 trials. Error bars are one standard error.
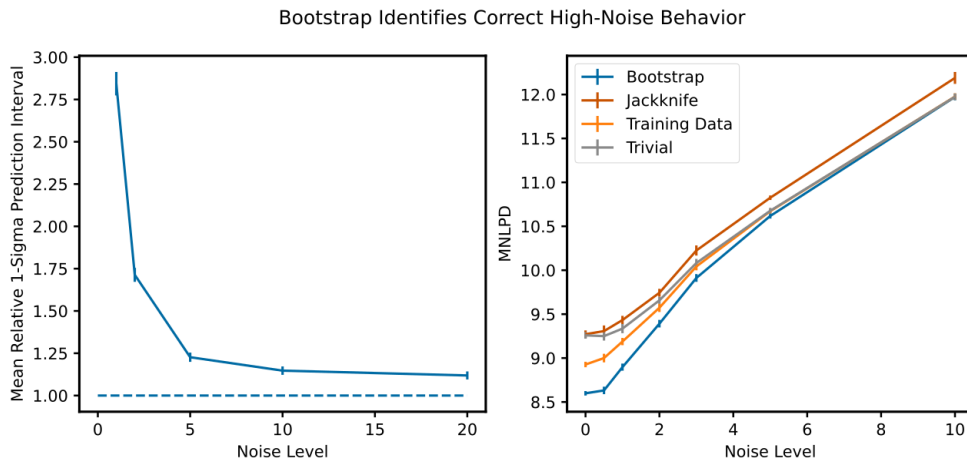
Figure 11: a) Recalibrated bootstrap prediction interval and b) MNLPD as the noise level varies for the Friedman-Grosse test problem. There are 128 training points, 64 bags, and 100 trials. Error bars are one standard error.